Research Square

Preprints are preliminary reports that have not undergone peer review.
They should not be considered conclusive, used to inform clinical practice,
or referenced by the media as validated information.

Spectroscopic Characterization and DFT Quantum Study of New Isoindigo Polymer: Promising Materials for High Optoelectronic Device Performance

M. Labiedh
University of Monastir, Avenue of Environment
A. Hfaiedh
University of Monastir, Avenue of Environment
A. Mabrouk
ali.mabrouk@isimm.rnu.tn
University of Monastir, Avenue of Environment
M. B. Braiek
University of Monastir, Avenue of Environment

Research Article

Keywords: Isoindigo, D-A structure, photophysical properties, TD-DFT, high-efficiency OSC

Posted Date: November 26th, 2026

DOI: https://doi.org/10.21203/rs.3.rs-11656314/v1

License: This work is licensed under a Creative Commons Attribution 4.0 International License.
Read Full License

Additional Declarations: No competing interests reported.

Spectroscopic Characterization and DFT Quantum Study of New Isoindigo Polymer: Promising Materials for High Optoelectronic Device Performance

M. Labiedh[1], A. Hfaiedh[1], A. Mabrouk[1,2,*], and M.B. Braiek[1]

[1]University of Monastir, Research Laboratory of Asymmetric Synthesis and Molecular Engineering of Organic Materials for Organic Electronic (LR18ES19), Department of Physics, Faculty of Sciences of Monastir, Avenue of Environment, Monastir, 5019, Tunisia.
[2]University of Monastir, Higher Institute of Computer Sciences and Mathematics of Monastir, Monastir, 5019, Tunisia.
*Corresponding author: Adress: Higher Institute of Computer Sciences and Mathematics, Avenue of Cornich, Monastir 5019, Tunisia.
Phone: +216 73464167; fax: +216 73464288
E-mail address: ali.mabrouk@isimm.rnu.tn

Abstract

In this work we deal with the synthesis, structural photovoltaic properties and quantum chemical modeling of new low band gap isoindigo-based polymer, derived from electron-accepting isoindigo units and several electron-donating groups, for renewable energy technologies and applications. The first isoindigo derivative polymer denoted as PPID were obtained in moderate heck reaction followed by photocyclodehydrogenation. As part of our analysis, the resulting polymer was characterized by thermal (ATG), cyclic voltammetry (CV), UV-Vis absorption and photoluminescence spectroscopies. The obtained polymer possesses good solubility in common organic solvents, high thermal stability, and broad absorption in the range of 300 to 750 nm. Some fundamental DFT/B3LYP/6-31G(d,p) calculated parameters matched well the experimental measurements, showing good structure-properties correlation. Then, a series of isoindigo-based donor polymers were systematically investigated where five new isoindigo-based polymers with a D-A structure were designed by engineering the donor groups in order to modulate their optoelectronic and charge-transport properties for use in photovoltaic device. Photophysical, electrochemical, and computational analyses were conducted to investigate the effect of donor units on the isoindigo-polymer derivatives. Their optoelectronic properties and other indispensable characteristic parameters were studied indicating that these D-A polymers can be promising active layer for organic solar cells (OSCs). These results not only provide a pathway for new polymer design but also serve as a theoretical foundation for future experimental development of high-efficiency electronic device.

Key words: Isoindigo, D-A structure, photophysical properties, TD-DFT, high-efficiency OSC.

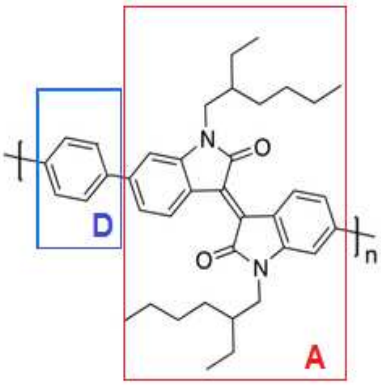
Highlights

- Numerous materials and various architectures have been developed for new isoindigo-based polymers.
- A remarkable intermolecular π−π stacking has been highlighted its potential in optoelectronic devices.
- Tuning of isoindigo-derivative optoelectronic properties by simply modifying the donor groups in D-A polymer systems.
- A spectroscopic characterization, quantum chemical DFT/B3LYP/6-31G(d,p) investigations and descriptors parameters were discussed.
- Explores flexible electronics, photovoltaics, and future research avenues.

1. Introduction

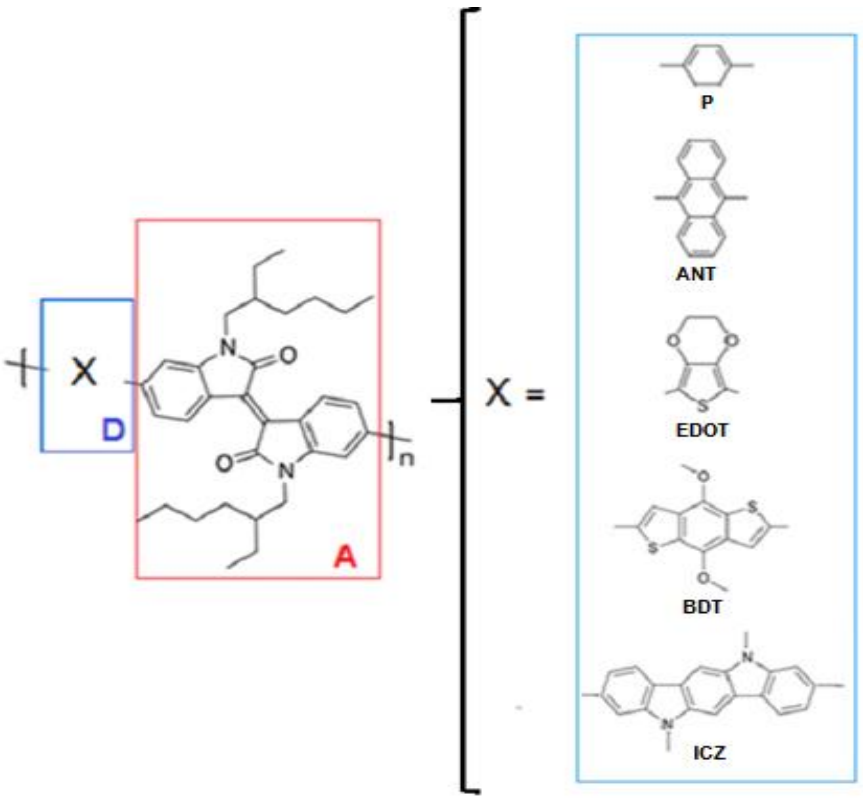
The properties and the characteristics of some new polymer architectures are fundamental to many advanced applications **[01–03]**. Generally, the physicochemical properties of these materials are often tailored to meet specific requirements, making their study crucial for technological advances in diverse fields, such as medicine, electronics and the environment **[04–06]**. Admittedly, these flexible materials offer a low-cost solution, and understanding their structure and behavior is essential for the development of sustainable, high-performance technologies **[07–09]**. Particularly, the materials used to design photovoltaic cells must promote π-stacking to increase mobility within the component where the oxidation potential must not be too low, so as to ensure good material stability and must also absorb across a broad range of the visible spectrum. In this context, isoindigo has proved to be an excellent electron-accepting building block for the synthesis of electroactive conjugated polymers with donor-acceptor structures exhibiting a remarkable optoelectronic property, thanks to its ease of large-scale synthesis and high yield **[10]**.

The isoindigo units has been found to be an excellent electron-accepting building block towards electroactive conjugated polymers with remarkable optoelectronic properties for organic electronics applications **[11]**. Although the application of isoindigo in organic electronics was first demonstrated by small molecules and the development of isoindigo-based polymers proved to be much faster **[12]**. Moreover, isoindigo with a symmetrical lactam structure, consisting of two indolin-2-one units, with strong electron-withdrawing character (with two carbonyl groups) has found modern applications in its conjugated organic polymer structures **[13–18]**. The central C=C double bond conjugated with two oxindole rings forms an extended π-conjugated structure **[19–21]** exhibiting excellent photochemical stability, facility in synthetic modification (with high reaction yields), with easy structural modification to achieve versatile acceptor materials **[22–24]**. Here we present a new polymer, named poly(phenylene-2,7-diyl-alt-[N,N′-(2-ethylhexyl)-isoindigo]-6′,6″-diyl), referred to as PPID (**Scheme 1**). In this work, we discuss the synthesis, the spectroscopic characterization and chemical quantum modelling for a better structure-property correlation of this isoindigo-polymer derivative.



Scheme 1. Chemical structure of the PPID polymer.

In this work, we discuss the synthesis, the spectroscopic characterization and quantum modelling to enable a better structure-property correlation for a new isoindigo polymer derivative. The chemical composition of these materials allows their properties to be modulated; we believe that a synergy of molecular engineering strategies applied to the donor units could further improve the performance and broaden the scope of application of isoindigo-based polymers **[25]**. Numerous materials and various architectures have been developed. In our study, six new multifunctional isoindigo-based electronic materials were designed and investigated (**Scheme 2**).



Scheme 2. Molecular structures of new polymers in D-A configuration structure.

Several electron-rich units have been identified, such as phenyl (P), anthracene (ANT), 3,4-ethylenedioxythiophene (EDOT), benzodithiophene (BDT) and indolocarbazole (ICZ). The resulting polymers are designed as PPID, PANTID, PEDOTID, PBDTID and PICZID, respectively. Generally, these electron-donating units give rise to dipole-dipole interactions and other π-π interactions within the polymer chains, which bring the polymer chains closer together, thereby promoting a well favorable structural organization **[26,27]**. In order to gain a better understanding of the properties of these structures, we naturally turned to quantum chemical approaches **[28]**. These organic polymers have been designed and theoretically investigated by DFT method at B3LYP/6-31G(d,p) level. Given the number of publications mentioned above, very few theoretical studies on this family of natural substances have been carried out to date. In fact, these theoretical calculations can provide insights into photophysical properties of these D-A polymers and allow us to establish clear structure-property relationships.

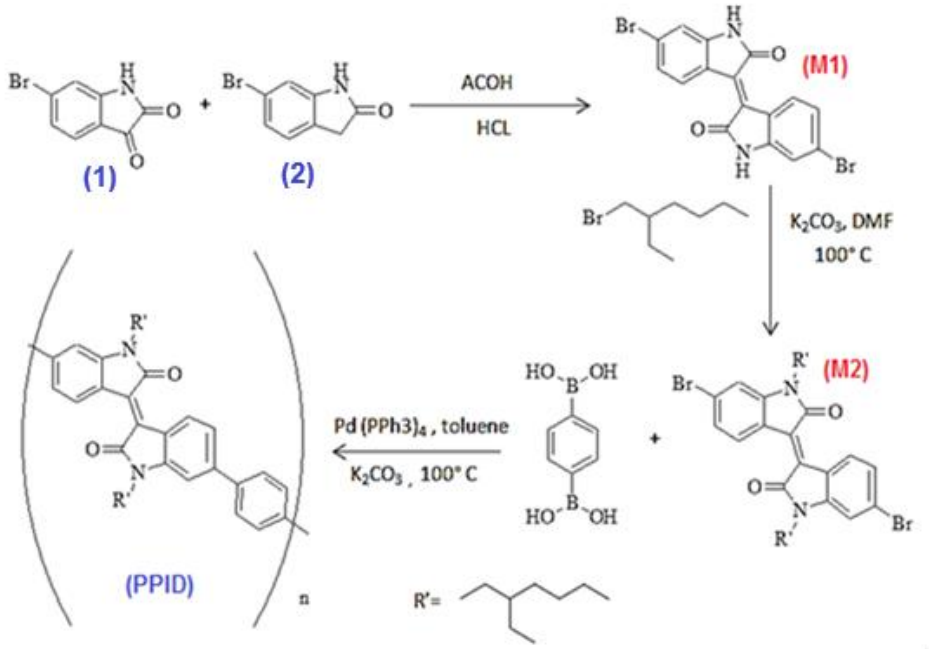
2. Material and characterization

Firstly, all the solvents, products and reagents designed for the synthesis were purchased from Aldrich. In the experimental section the Thermal gravimetric analysis (TGA) was carried out using a TA Instrument TGA Q500 instrument (heating rate of 10 °C min^{-1}). Then UV–Vis absorption spectra of the polymers was measured using Cary-300 UV–Vis spectrophotometer. The photoluminescence (PL) data were carried out in chloroform solution at room temperature, using an Agilent spectrophotometer equipped with a 450-W Xenon lamp. And the Cyclic Voltammetry (CV) was carried out in tetrabutylammonium hexafluorophosphate (0.1 M) as supporting electrolyte in acetonitrile and conventional three-electrode cell with a Pt working electrode, a platinum-wire counter electrode and an Ag/AgCl reference electrode was employed. The CV measurements were obtained on a CH-Instruments 650A Electrochemical Workstation.

2. Chemical structure and synthesis protocol

Initially, the starting material used in the syntheses was 6,6'-dibromoisoindigo. This compound (**M1**) can be easily prepared by the coupling of commercially available 6-bromooxindole (**1**) with 6-bromoisatin (**2**) in refluxing acetic acid and hydrochloric acid under nitrogen. Before being introduced into the polymerization reactions, each monomer was carefully purified. The synthetic routes of this polymer were described (**Scheme 3**).

$Pd_2(PPh_3)_4$ was used as a catalyst for the polycondensation reactions within the use of Sonogashira coupling mechanisms were the overall yield of PPID is high then 80%. The isoindigo core (**M1**) is almost insoluble in common organic solvents due to strong π-π stacking and intermolecular hydrogen bonding interactions arising from the hydrogen atoms on the lactam nitrogen's. For this reason, the introduction of long alkyl chains by substituting the hydrogens on the lactam nitrogen atoms can guarantee the solubility of the small molecules (**M2**) and the resulting polymers in common solvents **[29]**.



Scheme 3. Synthetic pathway of the target PPID polymer.

3.2. Modelling and calculation method

The molecular structures of all organic compounds under study were obtained from an unconstrained optimization of all geometrical parameters using the nonlocal hybrid Becke three-parameter Lee-Yang-Parr (B3LYP) functional **[30]** and a flexible with the 6-31G(d,p) basis set for all atoms in the polymeric skeleton (C, H, N, O). In fact, we performed density functional theory calculations with Gaussian 16 software package **[31]**. We have followed the same methodologies described in literature to ensure the accuracy of our calculations where the first 20 singlet excited-states were calculated with TD-DFT/B3LYP/6-31G(d,p) method **[32]**. Moreover, frequency calculations, at the same level of theory, were carried out for all systems and real frequencies were obtained, which confirms that all of them were minimum energy structures on the potential energy surface **[33]**. Based on the GaussSum program, the

optimized ground-state equilibrium geometries were used to calculate the distribution of the total density of states (DOS) for these organic systems **[34]**. Chemical potential, hardness and other chemical reactivity parameters were calculated and discussed.

3. Spectroscopic analysis and DFT modeling characterization

3.1. Thermal stability

The thermal stability of PPID which is of crucial importance for the preparation of the electronic device was investigated by themogravimetric analysis (TGA) (**Figure 1**). The resulting polymer showed very good thermal stability with an onset of decomposition temperature (T_d) at ~430°C. This graph shows the mass loss of the polymer versus increasing temperature (black curve) and the rate of change of this mass (red curve). The material is thermally stable up to approximately 350°C. The main degradation occurs at approximately 350°C. Beyond 400°C, the loss slows, indicating thermally resistant remnants. The total loss is approximately 45%, showing that a significant fraction of the material does not decompose up to 800°C. Its derivative, DTG (derivative thermogravimetry), represents the rate of mass loss, facilitating the precise identification of degradation stages.

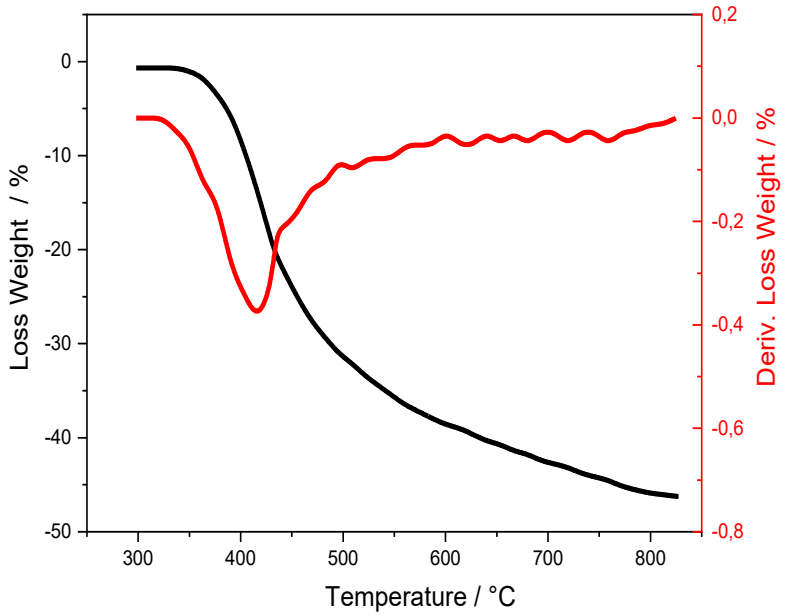


Figure 1. Themogravimetric analysis (TGA) of the PPID polymer.

3.3. Conformational and structural behavior

Conformational studies of the geometrical organic systems are crucial for designing high-performance active layer for organic electronic devices manufacture **[35]**. For this reason, we considered it useful to begin with a conformational study of the structure shown below (**Figure 2**).

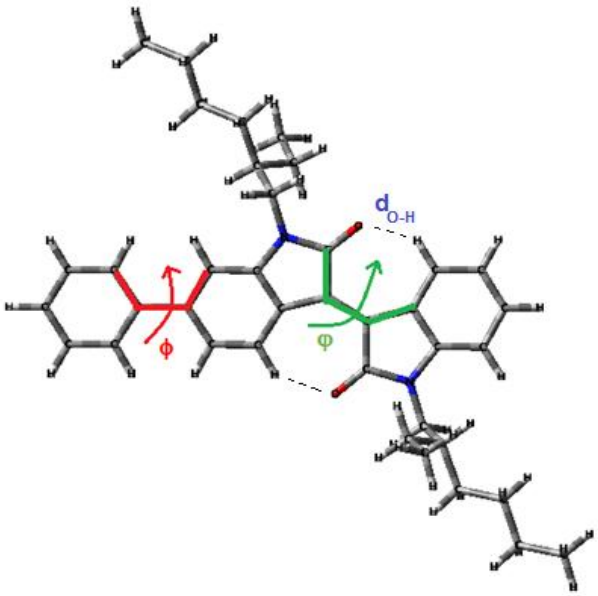


Figure 2. Conformational study of the PID monomer (with 20° increments).

Isoindigo unit consists of two indolin-2-one units fused via a central double bond. This central carbon–carbon double bond confers remarkable structural rigidity to the entire backbone. A slight twist (φ = 10° to 30°) is often observed due to steric hindrance between the carbonyl oxygen atoms and the adjacent hydrogen's of the conjugated ring O---H (d_{O---H} = 2.01 Å). The potential energy curves for the PID monomer are plotted by varying the torsion angle between the donor and acceptor units (ϕ) from 0 to 180°, in 20° increments. These calculations are performed using different bases for the sake of comparison.

From **Figure 3**, it can be seen that the potential energy curves for DFT/6-31G(d), 6-31G(d,p) and 6-311G(d,p) are very similar. Indeed, the torsion angles at which the energy is at a minimum are calculated to be identical, and the rotational barriers are very close. Furthermore, the overall shape of the curves obtained from DFT calculations using the 6-31G(d,p) basis set is similar to those obtained using the more extensive 6-311G(d,p) basis set. It should also be noted that only the intensity maxima are shifted by approximately 2 $k.cal.mol^{-1}$, depending on the used basis set. An examination of the potential energy leads us

to consider the 6-31G(d,p) basis set as the minimum level required for the conformational study of PPID and its derivatives.

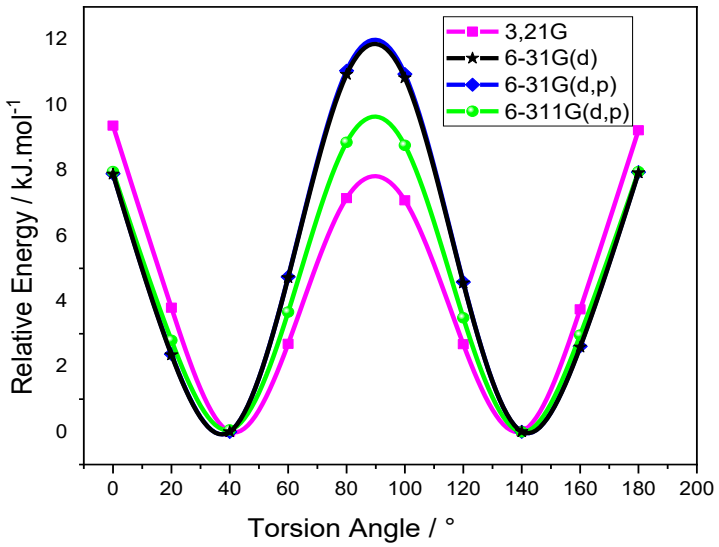


Figure 3. Potential Energy Surfaces (PES) calculated with B3LYP functional using different basis sets (from 3-21G to 6-311G(d,p).

The geometric structure results from a compromise between the electronic conjugation between the phenyl rings and steric effects leading to stable twisted shape. The most stable conformations correspond to torsion angles ϕ of 40° and 140°, respectively as illustrated in **Figure 4**.

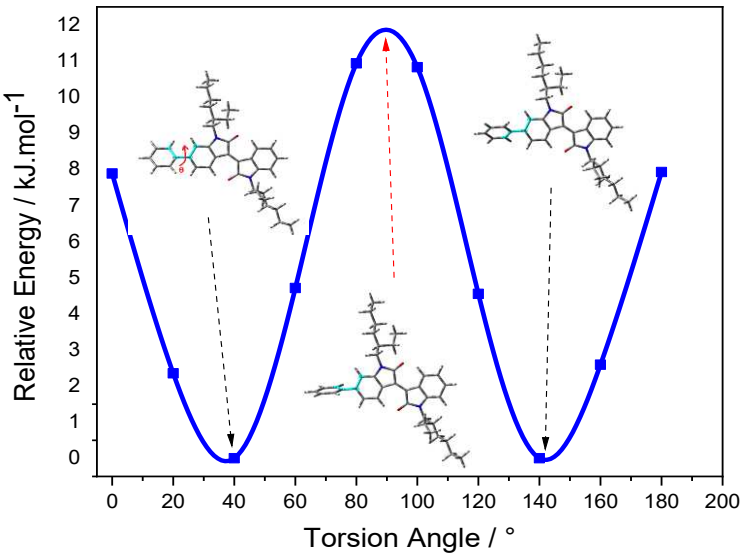


Figure 4. Illustration of the characteristic conformations of PPID in relation to the torsion angle ϕ.

3.4. Structural and photophysical properties

The geometry structure of the reference polymer (R≡PPID) was optimized in the chloroform solution using the DFT/B3LYP/6-31G(d,p) method, which had previously been considered to be the most appropriate computational method. Based on this validation, the same function was used to optimize all the polymers under investigation.

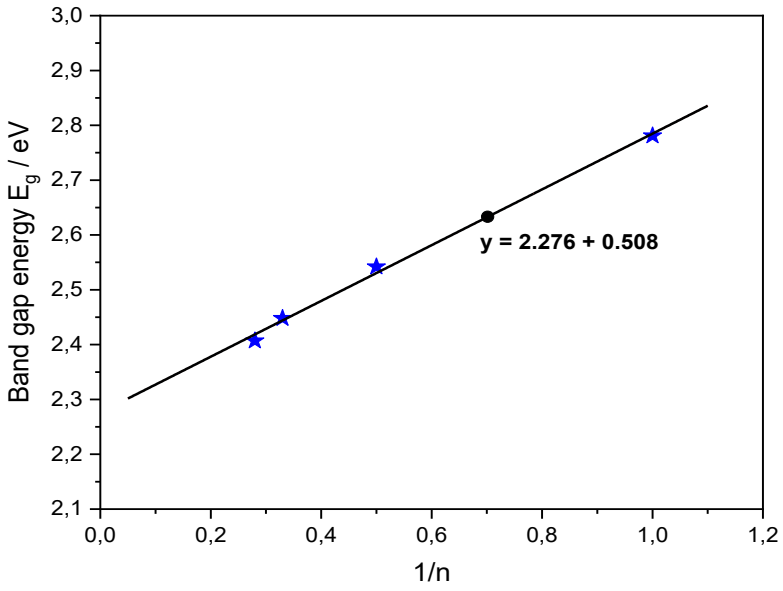


Figure 5. The simulated band gap energy E_g (E_{HOMO}-E_{LUMO}) for different monomer units is plotted against the inverse of the number of monomer units (n = 1 to 4).

Figure 5 shows the simulated estimate of the E_g gap energy for different monomer units, plotted against the inverse of the number of monomer units (1/n). this linear extrapolation show that the E_g gap of the PPID decreases as the number of monomers (n) increases to correspond to an E_g of about 2.27 eV.

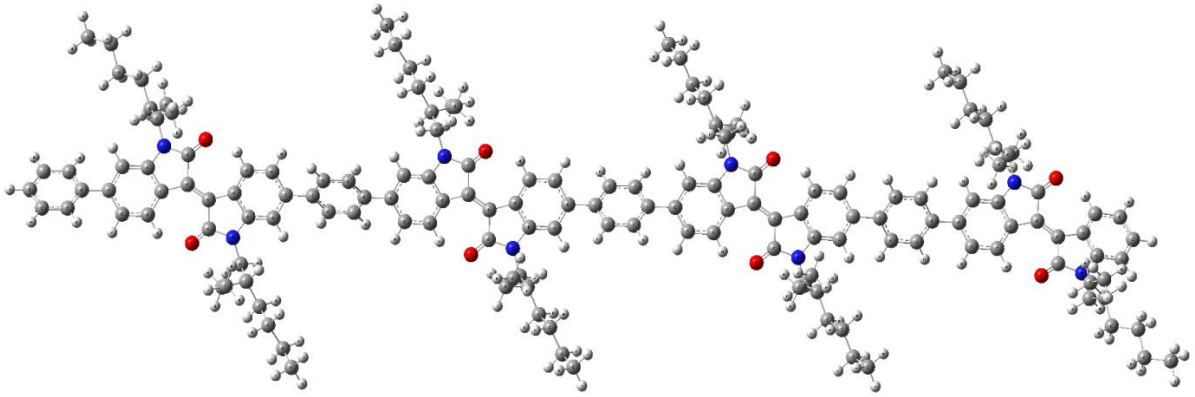


Figure 6. Fully optimised structure of $(PPID)_n$ (n = 4) using the DFT/B3LYP/6-31G(d,p) method.

Figure 6 illustrates the stable configuration of the PPID polymer. The optimized geometrical parameters were computed showing that the characteristic distances between terminal donor and acceptor groups range from 1.482 to 1.480 Å, values that lie between

those of single C–C bonds (1.540 Å) and double C=C bonds (1.340 Å). This intermediate bond length suggests the presence of a delocalized π-conjugation along the molecular backbone, as indicated by the torsion angles. The PPID polymer, whose donor unit is phenyl and whose acceptor unit is isoindigo, exhibits a non-planar backbone (ϕ = 35°) in its optimal conformation.

3.5. Electrochemical study (VC)

The supporting electrolyte used in this experiment was a 0.1 m solution of tetrabutylammonium hexafluorophosphate (Bu_4NPF_6) in anhydrous acetonitrile saturated with nitrogen. Platinum wires were used for the auxiliary electrode e. Ag/Ag^+ served as the reference electrode. For this polymer, cyclic voltammograms were recorded at a scan rate of 150 $mV \cdot s^{-1}$, as shown in **Figure 7**.

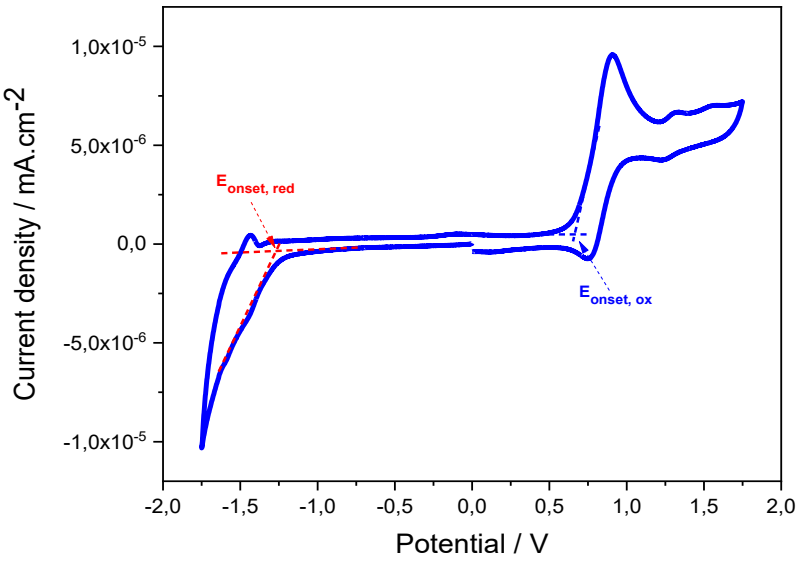


Figure 7. Cyclic voltammogram of PPID in CH_2Cl_2 solution (10^{-3} M) with 10^{-3} M $TBAPF_6$ at room temperature (at a scan rate 150 mV/s).

It is possible to deduce the HOMO and LUMO energy levels from the onset of oxidation and reduction, respectively. Each material exhibits two successive, quasi-reversible reduction and oxidation peaks relative to Ag/Ag^+. The potentials were referenced to the ferrocene/ferrocenium (F_c/F_c^+) redox couple.

$$E_{HOMO} = - (E_{onset,\ ox} - E^{0}_{Fc^{+}/Fc} + 4.89)\ eV$$

$$E_{LUMO} = - (E_{onset,\ red} - E^{0}_{Fc^{+}/Fc} + 4.89)\ eV$$

$$E_g^{elec} = (E_{LUMO} - E_{HOMO})\ eV$$

Furthermore, the oxidation onset potential ($V_{onset,\ ox}$) was measured at + 0.69 V, while the reduction onset potential ($V_{onset,\ red}$) is of the order of - 1.28 V. The HOMO and LUMO energy levels of PPID were determined from these values using the previous empirical relations where $E^{0}_{Fc^{+}/Fc}$ denotes the half-wave potential of ferrocene (0.42 V), measured relative to a saturated calomel electrode (Ag/AgCl). The energies of the HOMO and LUMO levels were estimated at - 5.16 eV and - 3.19 eV respectively, resulting in an electrochemical gap (E_g^{el}) of 1.97 eV, compared with the value of 2.27 eV obtained from DFT/B3LYP/6-31G(d,p) calculations (**Table 1**).

Optical			**Electrochemical** $E^{0}_{Fc^{+}/Fc}$= 0.42				
λ_{max}^{ABS} **(nm)**	λ_{max}^{EM} **(nm)**	E_g^{opt} **[eV][b]**	$E_{onset,red}$ **[V]**	$E_{onset,ox}$ **[V]**	E_{LUMO} **[eV][a]**	E_{HOMO} **[eV][a]**	E_g^{elec} **[eV][a,d]**
560	750	1.85	-1.28	0.69	-3.19	-5.16	1.97 (2.27)

- [a] *From the onset of oxidation and reduction processes: All potentials are referenced to the F_c/F_{c+} couple as internal standard.*
- [b] *From the long-wavelength absorption edge in $CHCl_3$ solution.*
- [c] *Values calculated by DFT method.*

Table 1. The corresponding optoelectronic data of PPID compound.

3.6. UV/Vis absorption and emission properties

The optical properties of this polymeric structure play a decisive role in the photovoltaic performance of OSCs **[36]**. The optical properties of PPID were investigated using UV/Vis absorption analyses on a diluted chloroform ($CHCl_2$) solution (10^{-5} M) using a Perkin UV-Vis spectrophotometer and the emission data were also recorded using an Elmer Lambda. We note that the polymer under investigation exhibits primarily a two-peak optical profile, which is common to conjugated polymers **[37]**. The UV-Vis spectra of the compounds showed strong absorption in the 350–470 nm regions. This absorption band is associated with π–π∗ electronic transitions **[38]** and is similar to the characteristic vibrational profiles of other isoindigo derivatives **[39]**. Some broad absorption bands have been observed in the low-energy region. Furthermore, the observation of absorbance peaks at 550 nm corresponds to the occurrence of intramolecular charge transfer (ICT) (from electron donors to electron

acceptors). The optical bandgap (E_g^{opt}) of PPID was calculated to be 1.85 eV based on the intersection between the absorption spectrum (UV-visible) and the emission spectrum (**Figure 8**). This approach allows the bandgap width to be determined whilst minimizing the stokes effect **[40]**.

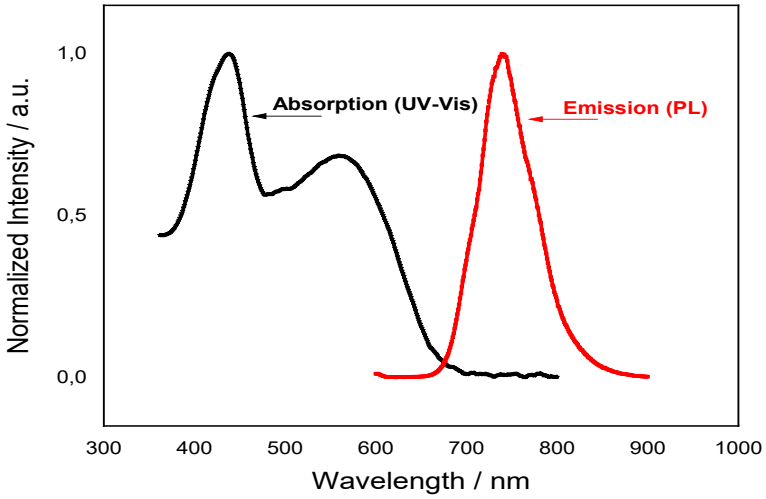


Figure 8. UV-Vis absorption and emission spectra of PPID polymer.

In this section, we examine the photoluminescence properties of the polymer under study. The data relating to the emission maximum are presented in **Table 2**. It can be seen that distinct photoluminescence spectra are observed, with an emission band when excited at 750 nm. A summary of the optical data from the TD-DFT calculations is presented here, along with the experimental measurements of the absorption and emission maxima (λ_{max}^{ABS}, λ_{max}^{EM}). It should be noted that the results reveal a difference of approximately 0.18 eV between the electrochemical bandgap (E_g^{elc}) and the optical bandgap (E_g^{opt}). This discrepancy can be attributed to the interfacial barrier between the electrode and the PPID, as well as to the energy required to dissociate the electron-hole pair (exciton) generated upon light absorption. Molecular orbitals are also fundamental descriptors used to study charge transfer, molecular interactions and electron distribution, particularly in the design of organic optoelectronic materials **[40]**. Indeed, the spatial distribution of molecular orbitals (**Figure 9**) shows that the electron density of the HOMO orbital extends across the entire chain **[42]**. Whereas that of the LUMO orbital is mainly localized on the isoindigo units due to the weak interaction between the two blocks. Furthermore, LUMO+2 orbital densities become quite strongly confined on the isoindigo units.

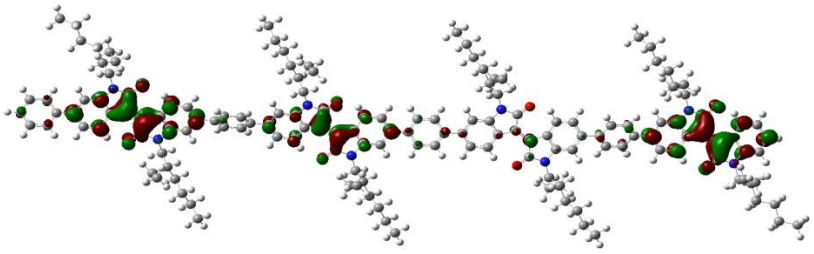
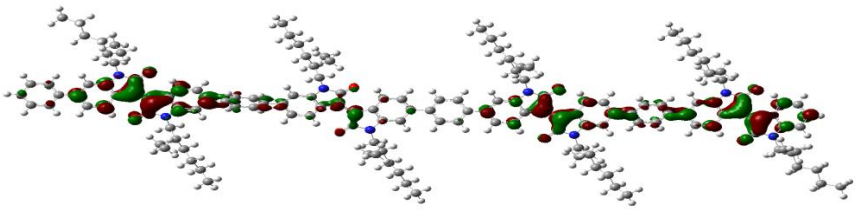
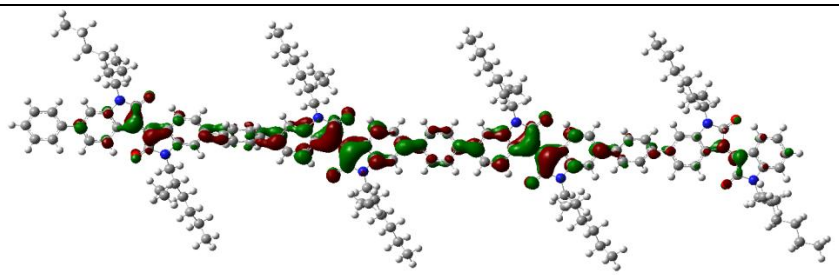
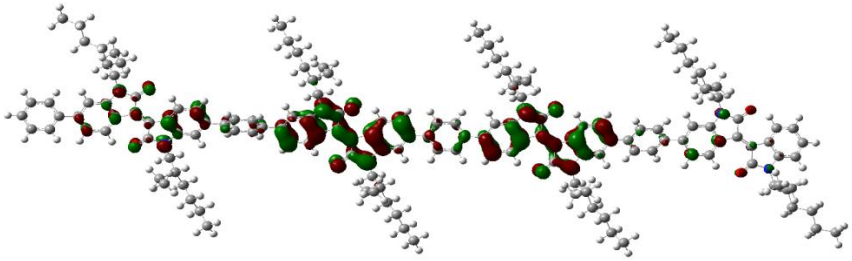
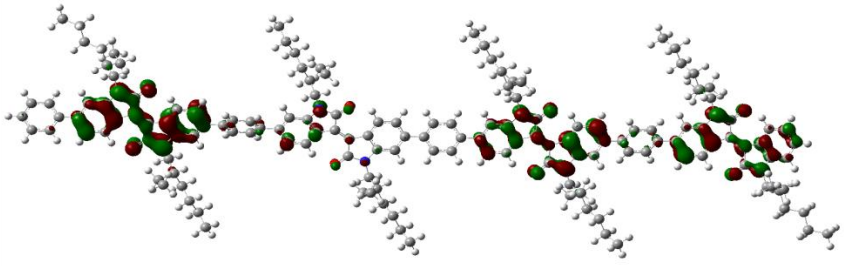
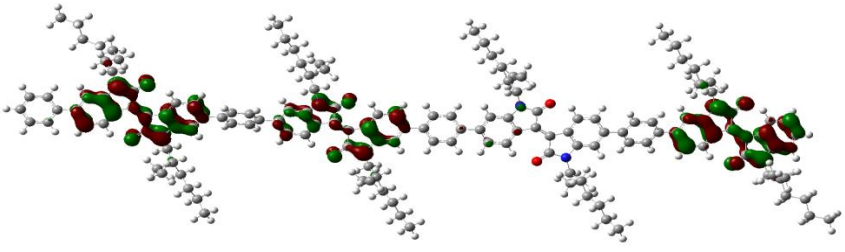
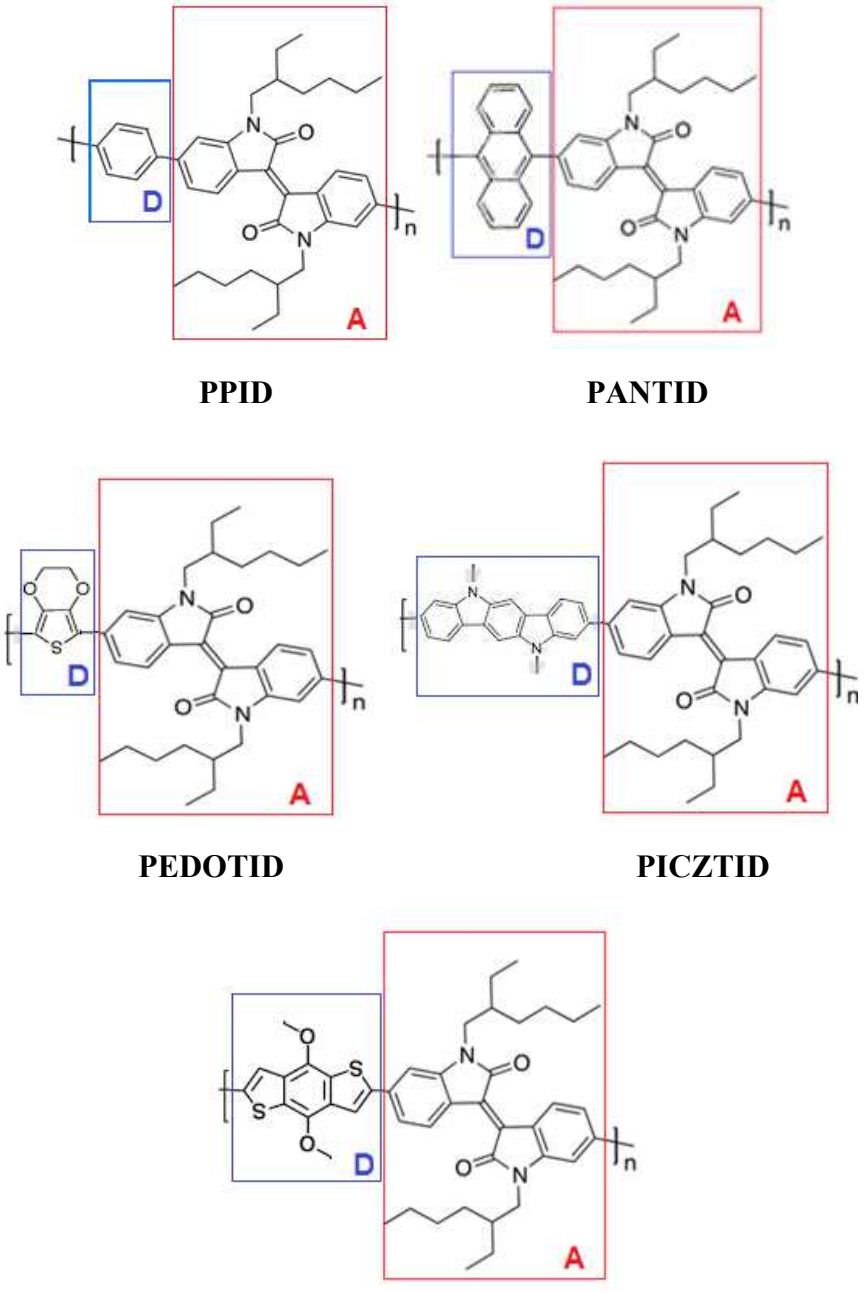
	Contour plots of FMO
LUMO+2	
LUMO+1	
LUMO	
HOMO	
HOMO-1	
HOMO-2	

Figure 9. Contour plots of the HOMO-n and LUMO+n molecular orbitals (n = 0, 1 and 2) of the PPID polymer.

4. New isoindigo-based polymers

4.1. Molecular design

The structure of the reference polymer (PPID) was structurally modified by introducing various electron-donating groups. These modifications resulted in five new derivatives (PPID–PBDTID). Consequently, all the polymers designed follow a Donor–Acceptor $(D–A)_n$ configuration, as illustrated in **Scheme 4.**



PBDTID

Scheme 4. Chemical structures of the designed polymers.

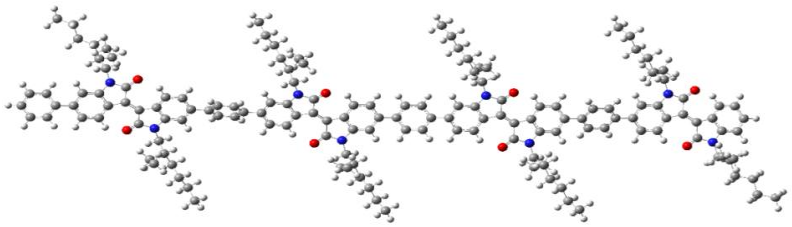
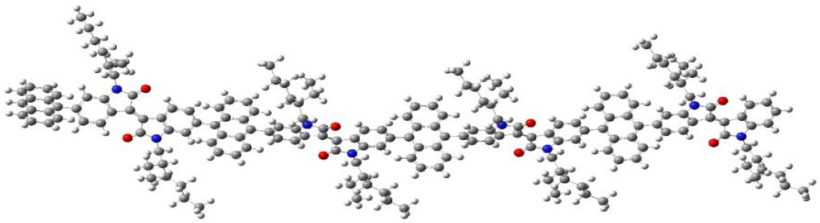
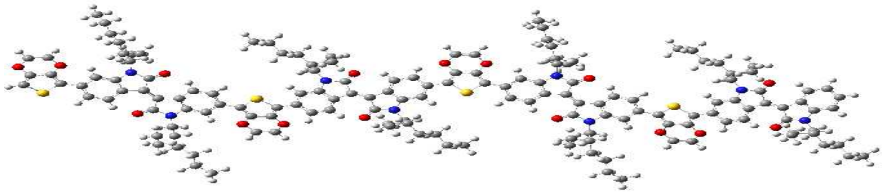
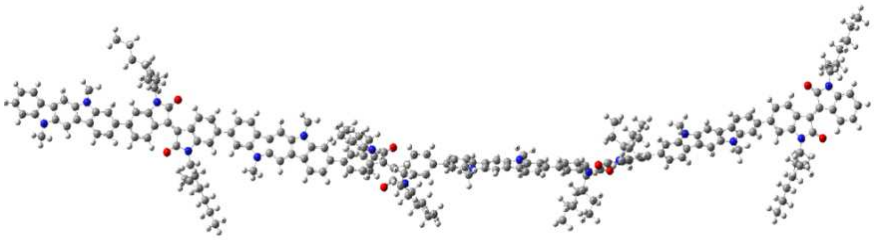
The photoelectric properties are strongly influenced by the bond lengths and dihedral angles of the molecular structure **[43]**. The bond lengths and angles between the donor and acceptor units were analysed on the basis of the optimised geometries of the molecules in order to better understand their structural organisation and electronic interactions. The corresponding values are summarised in the table below (**Table 2**). A smaller dihedral (torsion) angle generally corresponds to a more planar conformation, which promotes better delocalisation of π electrons and enhances conjugation. The lowest torsion angle is observed for PEDOTID and PBDTID, with a value of 20°, suggesting that they have the flattest configuration in the series. In this study, the molecular planarity parameter (MPP) and the amplitude of deviation from the plane (SDP) were used to quantitatively assess the geometric planarity of the designed polymers. A high MPP value corresponds to a greater deviation from planarity. Thus, a flatter configuration promotes efficient π–π stacking and enhances charge transport in OSCs. The SDP parameter quantifies the maximum vertical amplitude of atomic displacements relative to the fit plane and reflects the extent of local distortion. These geometric parameters are presented in **Table 2**.

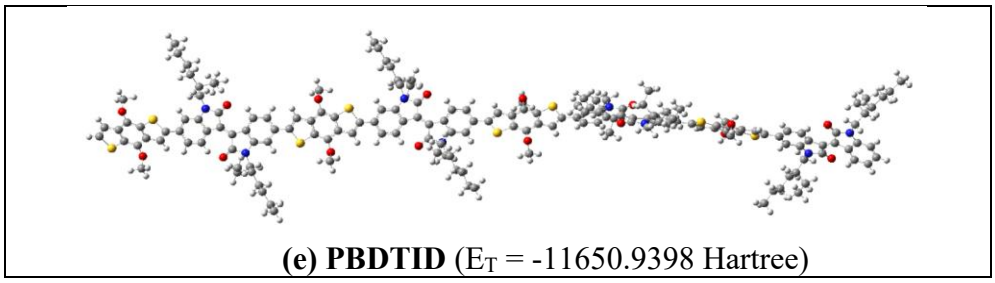
Polymer	Interatomic Distance L_{C-C} (Å)	Torsional Angle ϕ (°)	MPP (Å)	SDP (Å)
PPID	1.482	36.38	1.81	9.51
PANTID	1.495	75.55	2.28	11.02
PICZID	1.480	35.72	3.11	19.01
PEDOTID	1.459	18.36	1.94	10.23
PBDTID	1.463	21.71	1.78	9.31

Table 2. Structural parameters of the PPID and the designed polymers, derived from the optimized geometries.

The combination of MPP and SDP parameters is also a key factor in intermolecular interactions, charge delocalization and device performance. The lower the MPP and SDP values, the better the orbital overlap and the higher the charge carrier mobility, and consequently the higher the photovoltaic efficiency. The MPP values calculated for the reference polymer and the designed polymers are 1.81, 2.28, 3.11, 1.94 and 1.78 Å respectively. The PBDTID polymer has the lowest MPP value, indicating superior structural

planarity. In contrast, the PICZTID polymer has the highest MPP value, suggesting greater torsion within its molecular backbone. The corresponding SDP values are 9.51, 11.02, 19.01, 10.23 and 9.31 Å, thus confirming the greater planarity of PBDTID compared with the other derivatives (**Figure 10**).

Designed polymer (E_T)
 **(a) PPID** (E_T = -6939.5525 Hartree)
 **(b) PANTID** (E_T = -8168.6235 Hartree)
 **(c) PEDOTID** (E_T = -9129.2572 Hartree)
 **(d) PICZTID** (E_T = -9536.0528 Hartree)



(e) PBDTID (E_T = -11650.9398 Hartree)

Figure 10. Representation of the optimized structures of the designed polymers ((a): PPID, (b): PANTID, (c): PEDOTID, (d): PICZID and (e): PBDTID) using the DFT/B3LYP/6-31G(d,p) method.

4.2. Characteristic optoelectronic parameters

The optical properties of these organic systems with D-A structures play a decisive role in the photovoltaic performance of organic solar cells (OSCs). Parameters relating to excited states are now commonly used to study the underlying mechanisms of photocurrent generation and their relationship with spectral characteristics **[44]**. The simulated absorption spectra of PPID and the polymers designed using the TD-DFT/B3LYP/6-31G(d,p) method are shown in **Figure 11**.

It should be clearly noted that all the polymers developed are characterized by absorption spectra that are broader than that of PPID. These materials exhibit significant absorption in the visible and near-infrared regions, demonstrating their high potential for efficient photon collection in the target region of the solar spectrum, specifically PBDTID, with PEDOTID and PICZID having good molar absorptivity's > 1.5×10^5 $M^{-1}.cm^{-1}$. The oscillator strength (*f*), dipole moment (μ_D) and maximum absorption wavelength (λ_{max}^{ABS}) are also recorded for these compounds (**Table 3**).

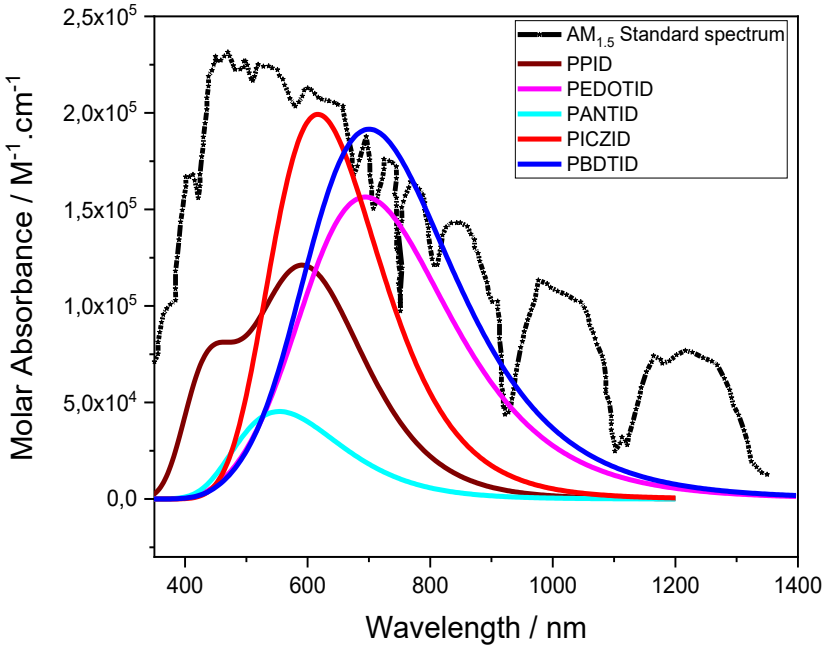


Figure 11. Representation of the optimised structures of the designed polymers ((a): PPID, (b): PANTID, (c): PEDOTID, (d): PICZID and (e): PBDTID) using the DFT/B3LYP/6-31G(d,p) method.

The λ_{max}^{ABS} values for PPID and the other polymers developed lie within the range of 545 to 710 nm. The spectra of two compounds, PEDOTID and PBDTID, show a red shift in absorption compared with PPID, whereas this is not the case for PANTID and PICZTID. The order of the λ_{max}^{ABS} values is as follows: PBDTID > PEDOTID > PICZTID > R≡PPID > PANTID. The most pronounced red shift is observed for PBDTID **(Table 3**).

	λ_{max}^{ABS} **(nm)**	f	**ε** **($M^{-1}cm^{-1}$)**	**MO (coefficient)**	**μ_D (Bebye)**
PPID	602	2.7195	1.21 10^5	HOMO →LUMO (78%)	1.13
PANTID	545	0.6298	0.45 10^5	HOMO-6 → LUMO +1 (28%)	0.62
PICZTID	618	4.1062	2.01 10^5	HOMO-2→ LUMO (21%)	2.27
PEDOTID	700	3.5781	1.57 10^5	HOMO→LUMO (78%)	2.63
PBDTID	710	4.2901	1.92 10^5	HOMO→LUMO (81%)	3.95

Table 3. Characteristic electronic parameters of the various polymers.

The value of λ_{max}^{ABS} is significantly influenced by modifications to the donor group in the main chain. The electron-donating effect is enhanced, which increases the λ_{max}^{ABS} values

of these materials and, consequently, reduces the band gap (E_g) by altering the HOMO and LUMO levels. By examining the electronic structures of these different polymers, as shown in **Figure 12**, a marked change in the arrangement of the electronic levels can be observed.

Similarly, the incorporation of thiophene slightly destabilizes these levels, allowing for lower E_g gaps. This demonstrates that the designed polymers exhibit increased absorbance compared to the PPID reference polymer, suggesting that they can present promising active materials for organic solar cells (OSCs). In fact, the electronic properties of these π-conjugated structures can certainly be modulated by the presence of conjugated units in the main chain or by the appropriate choice of donor groups.

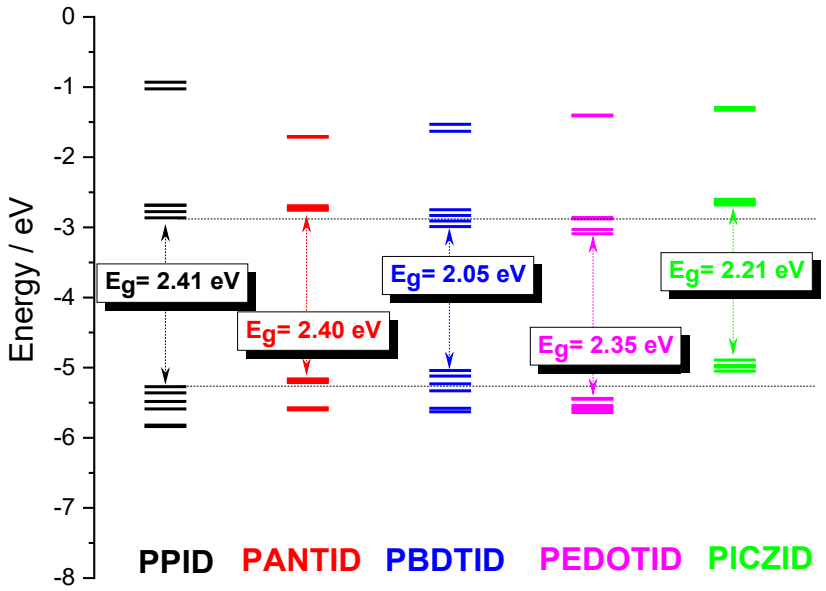


Figure 12: Electronic structure of the various polymers.

The calculated E_g^{elec} values, in descending order, are as follows: PBDTID (2.05 eV) < PICZTID (2.21 eV) < PEDOTID (2.35 eV) < PANTID (2.40 eV) < R≡PPID (2.41 eV). Generally, for these structures in the ground state, the HOMO is mainly delocalized over the donor core, whilst in the excited state, the LUMO becomes more localized over the terminal acceptor units. This spatial separation of the HOMO and LUMO confirms an efficient intermolecular charge transfer (ICT) upon excitation, which is a key characteristic of high-performance OSCs. The addition of donor motifs lowers the LUMO levels in PBDTID and

PEDOTID, in particular, those containing strong electron-donating groups result in a lower E_g compared with PPID.

The dipole moment (D) is a key parameter that reflects the degree of charge separation within a molecule and plays a vital role in determining molecular polarity, solubility and the effective transport behavior of charges between donor and acceptor units, and then significantly influences the device's performance. In this study, the dipole moments parameter of the designed polymers were calculated using the B3LYP/6-31G(d,p) method. The calculated values, summarized in **Table 3**, show that the ascending order of μ values is as follows: PANTID < PPID < PICZID < PEDOTID < PBDTID, and that PBDTID has the highest dipole moment, with a value of 3.95 Debye. This fact suggests firstly an ability to form uniform and stable active layers. Furthermore, a higher dipole moment may strengthen intermolecular interactions, promote better molecular packing and, consequently, facilitate intramolecular charge transfer (ICT) by encouraging self-assembly and crystallinity **[45]**.

The high dipole moment of PBDTID highlights its potential as an effective photoactive material for OSCs. Together, these characteristics result in better hole and electron mobility, well-suited donor-acceptor architecture and an enhanced form factor, which can be also translates into improved device performance.

4.4. Molecular electrostatic potential (MEP)

Electron density correlated with the molecular electrostatic potential (MEP) is an excellent descriptor for elucidating electrophilic and nucleophilic attack sites, the nature of charge separation, and intramolecular interactions **[46]**. This study is often correlated with dipole moments, electronegativity, partial charges and the chemical reactivity assess the optoelectronic behaviour of organic materials **[47]**. In this study, we carry out an MEP analysis of a series of polymers (PPID→PBDTID), based on the optimized molecular structure using the DFT/B3LYP/6-31G(d,p) method, as illustrated in **Figure 13**.

The electrostatic potential generally follows the gradient: red < yellow < green < cyan < blue, ranging from the most negative to the most positive potential. The MEP maps suggest that the central donor cores are predominantly marked by blue areas, while the terminal acceptor units exhibit red, yellow and light green areas. This pattern reflects a directional charge separation from the electron-donating core towards the electroattractive ends, which promotes efficient intermolecular electron transfer (ICT) upon excitation.

Of all the polymers designed, PBDTID exhibits the most pronounced red regions at the ends, which is attributed to the strongly electron-donating nature of the oxygen and sulphur atoms present in this donor group. These highly electronegative atoms draw the electron density towards the acceptor, enhancing charge separation and improving charge mobility. The MEP analysis also confirms that all the designed molecules exhibit effective charge separation and a favourable electron density distribution. This insight into electron distribution suggests that the polymers studied possess the characteristics of highly significant charge transfer, in particular, PBDTID, which has a higher electronegativity (-9.206 e^{-2} a.u.) and exhibits more pronounced ICT behaviour.

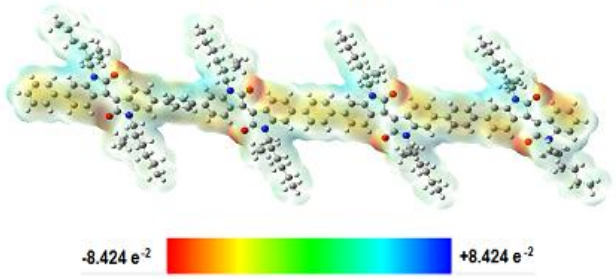
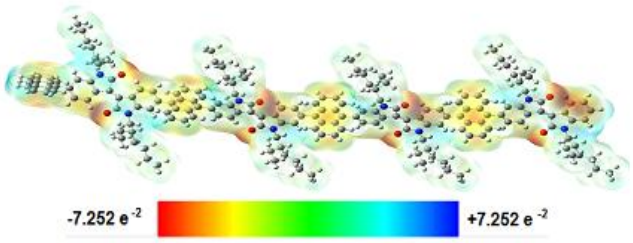
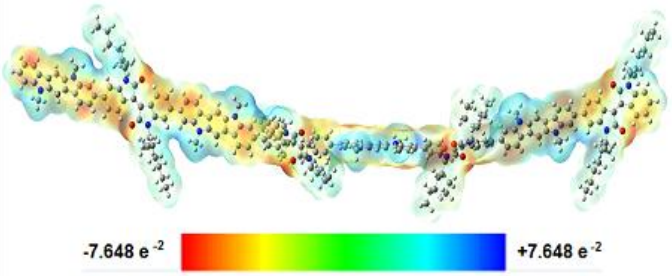
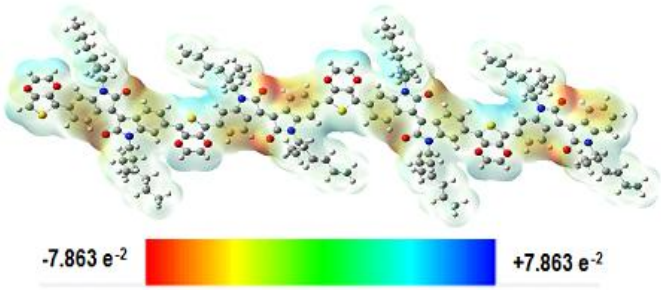
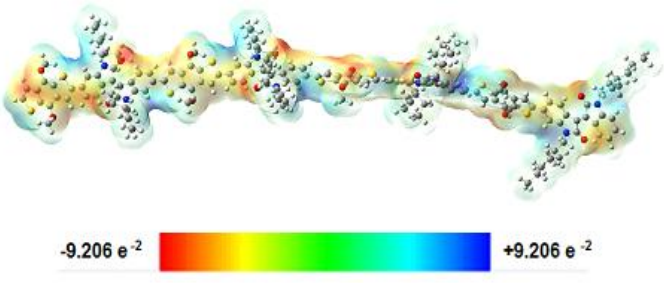
Polymer	Molecular electrostatic potential (MEP)
PPID	
PANTID	
PICZID	
PEDOTID	
PBDTID	

Figure 13. Molecular electrostatic potential (MEP) surfaces of the designed polymers (PPID-PBDTID), highlighting the regions of electron density distribution.

4.5. Chemical reactivity parameters

A number of quantum reactivity descriptors have now become a powerful tool for studying the organic reactivity of organic compounds and D-A-type polymeric systems. These characteristics are essential for understanding the injection and charge transport properties of active layer materials. Using the theorems of Parr and Pearson, these parameters including chemical hardness (η), softness (S), electronegativity (χ), chemical potential (μ) and electrophilicity index (ω) are related to the ionisation potential (IP) and electron affinity (EA) **[48–50]**.

$$\mu = (EA+IP)/2 \quad (1)$$

$$\eta = (IP-EA)/2 \quad (2)$$

$$\omega = \mu^2/2\eta \quad (3)$$

$$S = 1/\eta \quad (4)$$

$$\chi = -\mu \quad (5)$$

The analysis of the collected data presented in **Table 4** reveals that the PEDOTID and PBDTID derivatives exhibit relatively higher PI and AE values, indicating good electron-accepting capacity and better charge insertion capability. The IP values follow this order: R=PPID > PANTID > PBDTID > PEDOTID > PICZTID. Meanwhile, the EA values are ranked as follows: PBDTID > PEDOTID > R=PPID > PANTID > PICZTID. In general, molecules with a lower IP are chemically more flexible and more reactive, while those with a higher EA are stiffer and more stable. Similarly, higher η values correspond to chemically less reactive and structurally more stable polymers, while those with higher S values are more reactive and facilitate dynamic charge transfer processes.

The addition of donor motifs to the polymer chain reduces the hardness η from 1.40 eV (PICZTID) to 1.02 eV in the case of PBDTID. Generally, this parameter is used as a tool to measure charge transfer resistance to changes in its electronic configuration which is linked to the stability and the reactivity of the chemical system **[51]**. Furthermore, modifying the donor units increases electrophilicity (ω) in the following order: ωPICZTID < ωPANTID <ωR=PPID <ωPEDOTID <ωPBDTID. Moreover, these polymers are classified as super-electrophiles with electrophilities of $\omega \geq 4.00$ eV **[52]**. A comparative study of these polymers

indicates that PBTID has the highest softness (0.98 eV^{-1}), which improves charge transfer properties and enhances the material's polarizability. In the case of organic solar cells (OSCs), high flexibility (S) and reactivity promote intramolecular charge transfer (ICT) and exciton dissociation, and thus the performance of the device in question.

	EA (eV)	IP (eV)	η (eV)	S (eV^{-1})	χ (eV)	μ (eV)	ω (eV)
PPID	2.86	5.27	1.20	0.83	4.06	- 4.06	6.86
PANTID	2.75	5.16	1.21	0.82	3.95	- 3.95	6.44
PICZID	2.68	4.89	1.40	0.71	3.79	- 3.79	5.13
PEDOTID	3.09	5.44	1.17	0.85	4.26	- 4.26	7.75
PBDTID	3.00	5.04	1.02	0.98	4.02	- 4.02	7.92

Table 4. Chemical parameters of the D-A systems: chemical potential (μ), hardness (η), electronegativity (χ), softness (S) and electrophilicity index (ω), measured using the DFT/B3LYP/6-31G(d,p) method.

Electronegativity refers to a molecule's ability to donate electrons; the highest values are - 4.06 and - 4.02 eV for PPID and PBDTID, respectively. Furthermore, it is well known that a good electrophilic species has a high |μ| value and a low η value **[53]**. Overall the PBDTID polymer appears to be the most reactive, and all these parameters indicate that PBDTID is the most suitable material for the manufacture of electronic components.

4.6. State Density (DOS) Analysis

The study of density of states (DOS) enables the analysis of the distribution of energy levels within frontier molecular orbitals (FMOs). It provides valuable information on the electronic transitions and absorption characteristics associated with the various fragments of the polymeric structure. As illustrated in **Figure 14**, the DOS profiles clearly highlight the contribution of the donor units to the HOMO orbitals, whilst the LUMO orbitals are mainly localised on the electron-deficient isoindigo backbone, which also dictates the polymer's narrow optical bandgap. This significant contribution confirms their role in facilitating intramolecular charge transfer (ICT) in the main backbone polymer. The donor capacity of the benzodithiophene (BDT) and 3,4-ethylenedioxythiophene (EDOT) units, compared with the reference polymer (PPID), results in a significant reduction in the band gap energy (E_g). In particular, the incorporation of strong electron-donating units and the extension of conjugation in the designed polymers enhance their ability to modulate electron density, thereby improving charge separation and transport. DOS analysis validates the design strategy

aimed at strengthening the donor units in the newly developed polymer structures and in improving the optoelectronic properties and photovoltaic performances of such materials.

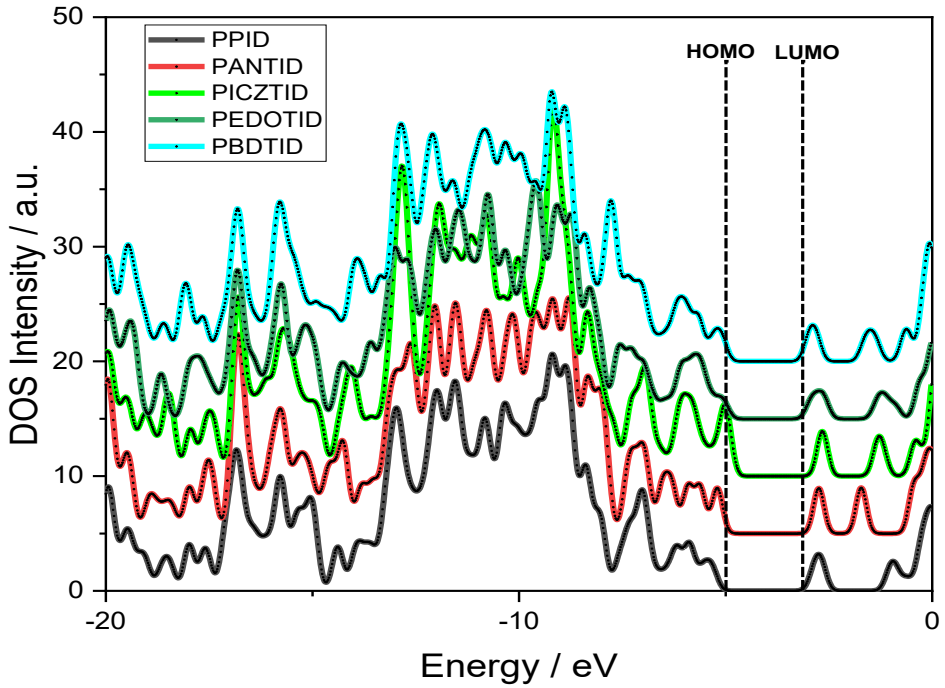


Figure 14. DOS spectra of the designed polymers (PPID→PBDTID), showing the contributions of the different donor units in the main backbone.

5. Conclusion

Through experimental characterizations and quantum DFT theoretical calculations we have described a comprehensive study of a π-extended isoindigo D-A polymer properties where we have firstly, target the polymer (R≡PPID) taken as a reference. This was achieved through in-depth experimental characterisation and theoretical DFT and TDDFT calculations. Then, we systematically investigated a series of isoindigo-based donor polymers where five new isoindigo-based polymers with a D-A structure were designed by engineering the donor groups in order to modulate their optoelectronic and charge-transport properties for use in photovoltaic device. This series of polymers differs only in its donor units, where they exhibit distinct morphological and electronic properties, which could result in significantly different device efficiencies.

The absorption spectra are shifted towards the red and there is improved alignment of the boundary orbitals. State density (DOS) analyses and molecular electrostatic potential (MEP) calculations have confirmed pronounced intramolecular charge transfer (ICT) and an

effective redistribution of electron density, promoting efficient charge separation in these polymeric systems. These computational results clearly demonstrate that a rational modification of the internal donor units, notably through the introduction of benzodithiophene (BDT) or 3,4-ethylenedioxythiophene (EDOT), can effectively enhance intramolecular charge transfer by suppressing charge recombination and then increasing the overall efficiency of the OSC device. This study of isoindigo-derivative polymer systems nicely illustrates how the electronic and optical properties of the polymer can be molecularly engineered by simply modifying the donor groups in D-A polymer systems. The data obtained are expected to contribute to the development of molecular engineering strategies towards further improving the performance and broadening the application of these organic materials.

Declaration of interests

The authors declare that there are no known conflicts of interest associated with this publication.

Declaration of AI Assistance

During the preparation of this work, the author(s) used ChatGPT to improve the language, style, and readability of the text. After using this tool, the author(s) reviewed and edited the content as needed and take(s) full responsibility for the content of the publication.

Author Contributions

M. Labiedh: Conceptualization, Characterizations, Writing and original draft preparation, A. Hfaiedh and A. Mabrouk: designed the proposed methods analyzed and validated the spectral data. A. Mabrouk and M.B. Braiek: analysed the data and reviewed and edited the draft. All authors have read and agreed to the published version of the manuscript.

Data availability

No data was used for the research described in the article.

References

[1] M. Helgesen, R. Sondergarrd, F.C. Krebs, Advanced materials and processes for polymer solar cell devices, J. Mater. Chem. 20 (2010) 36. https://doi.org/10.1039/b913168j.

[2] A.J. Mozer, N.S. Sariciftci, Conjugated polymer photovoltaic devices and materials, C. R. Chimie 9 (2006) 568.

https://doi.org/10.1016/j.crci.2005.03.033.
[3] M. Svensson, F. Zhang, S.C. Veenstra, W.J.H. Verhees, J.C. Hummelen, J.M. Kroon, O. Inganäs, M.R. Andersson, High-Performance Polymer Solar Cells of an Alternating Polyflourene Copolymer and a Fullerene derivative, Adv. Mater. 15 (2003) 988. https://doi.org/10.1002/adma.200304150.
[4] J.F. Lee, S.L.C. Hsu, P.I. Lee, H.Y. Chuang, M.L. Yang, J.S. Chen, W.Y. Chou, A new intramolecular donor–acceptor polyfluorene copolymer for bulk heterojunction solar cells, Solar Energy Materials & Solar Cells 94 (2010) 1166. https://doi.org/10.1016/j.solmat.2010.03.002.
[5] Y.W. Li, L.L. Xue, H. Li, Z.F. Li, B. Xu, S.P. Wen, Energy level and molecular structure engineering of conjugated donor-acceptor copolymers for photovoltaic applications, Macromolecules 42 (2009) 4491. https://doi.org/10.1021/ma900623p.
[6] C.J. Brabec, N.S. Sariciftci, J.C. Hummelen, Plastic solar cells. Advanced Functional Materials 11 (2001) 128. https://doi.org/10.1002/1616-3028 (200102)11:1<15::AID-ADFM15>3.0.CO;2-A.
[7] A. Azazi, A. Mabrouk and K. Alimi, Theoretical investigation on the photophysical properties of low-band-gap copolymers for photovoltaic devices, Computational and Theoretical Chemistry 978 (2011) 7. https://doi.org/10.1016/j.comptc.2011.08.020.
[8] S. Khan, A. Iqbal, Organic polymers revolution: Applications and formation strategies, and future perspectives, Journal of Polymer Science and Engineering 6 (2023) 3125. https://doi.org/10.24294/jpse.v6i1.3125.
[9] R.N.D. Niță, S. Frąckowiak, An Overview of Potential Applications of Environmentally Friendly Hybrid Polymeric Materials, Polymers 17 (2025) 252. https://doi.org/10.3390/polym17020252.
[10] L.H. Slooff, S.C. Veenstra, J.M. Kroon, D.J.D. Moet, J. Sweelssen and M.M. Koetse, Determining the internal quantum efficiency of highly efficient polymer cells through optical modeling, Applied Physics Letters 90 (2007) 143506. https://doi.org/10.1063/1.2718488.
[11] J. Mei, K.R. Graham, R. Stalder, J.R. Reynolds, Synthesis of isoindigo-based oligothiophenes for molecular bulk heterojunction solar cells, Org. Lett. 12 (2010) 660. https://doi.org/10.1021/ol902512x.
[12] H. Gu, S. Ming, K. Lin, S. Chen, X. Liu, B. Lu, J. Xu, Isoindigo as an electron−deficient unit for high-performance polymeric electrochromics, Electrochimica Acta 260 (2018) 772. https://doi.org/10.1016/j.electacta.2017.12.033.
[13] E.G. Wang, Z.F. Ma, Z. Zhang, K. Vandewal, P. Henriksson, O. Inganas, et al. An easily accessible isoindigo-based polymer for high-performance polymer solar cells, J. Am. Chem. Soc. 133 (2011) 14244. https://doi.org/10.1021/ja206610u.
[14] Y. Rout, V. Chauhan, R. Misra, Synthesis and characterization of isoindigo-based push–pull chromophores, J. Org. Chem. 85 (2020) 4611. https://doi.org/10.1021/acs.joc.9b03267.
[15] G. Zhang, Y. Dai, Y. Liu, J. Liu, H. Lu, L. Qiu, et al., Facile green synthesis of isoindigo-based conjugated polymers using aldol polycondensation, Polym Chem. 8 (2017) 3448. https://doi.org/10.1039/C7PY00484B.

[16] R.S. Ashraf, A.J. Kronemeijer, D.I. James, H. Sirringhaus, I. McCulloch, A new thiophene substituted isoindigo based copolymer for high performance ambipolar transistors, Chem Commun. 48 (2012) 3939. https://doi.org/10.1039/c2cc30169e.

[17] T. Lei, J.Y. Wang, J. Pei, Design, synthesis, and structure-property relationships of isoindigo-based conjugated polymers, Accounts of Chemical Research 47 (2014) 1117. https://doi.org/10.1021/ar400254j.

[18] N.M. Randell, T.L. Kelly, Recent advances in isoindigo-inspired organic semiconductors, Chem. Rec. 19 (2019) 973-988. https://doi.org/10.1002/tcr.201800135.

[19] S. Li, J. Yuan, P. Deng, W. Ma, Q. Zhang, A comparative study of diketopyrrolopyrrole and isoindigo based polymers for organic photovoltaic applications, Dyes Pigments 106 (2014) 121. https://doi.org/10.1016/j.dyepig.2014.03.002.

[20] W. Ying, F. Guo, J. Li, Q. Zhang, W. Wu, H. Tian, et al., Series of new D-A-π-A organic broadly absorbing sensitizers containing isoindigo unit for highly efficient dye-sensitized solar cells, ACS Appl. Mater. Interfaces 4 (2012) 4215. https://doi.org/10.1021/am300925e.

[21] M. Shaker, H. Hayashi, H. Yamada, Molecular organized isoindigo based small molecules with terminal thermally cleavable protecting group, Dyes Pigments 184 (2021) 108806. https://doi.org/10.1016/j.dyepig.2020.108806.

[22] A.V. Bogdanov, V.F. Mironov, Recent advances in the application of isoindigo derivatives in materials chemistr, Beilstein J. Org. Chem. 17 (2021) 1533. https://doi.org/10.3762/bjoc.17.111.

[23] H. Dinçalp, G.M. Saltan, C. Zafer, A. Mutlu, Synthesis and photophysical characterization of isoindigo building blocks as molecular acceptors for organic photovoltaics, Spectro. Chim. Acta. Mol. Biomol. Spectrosc. 202 (2018) 196. https://doi.org/10.1016/j.saa.2018.05.048.

[24] R. Stalder, J. Mei, K.R. Graham, L.A. Estrada, J.R. Reynolds, Isoindigo, a versatile electron-deficient unit for high-performance organic electronics, Chem. Mater. 26 (2014) 664. https://doi.org/10.1021/cm402219v.

[25] T. Lei, J.-Yu Wang, J. Pei, Design, Synthesis, and Structure–Property Relationships of Isoindigo-Based Conjugated Polymers, Acc. Chem. Res. 47 (2014) 1117. https://doi.org/10.1021/ar400254j.

[26] R.T. Kahl, A. Erhardt, G. Krauss, F. Seibold, O. Dolynchuk, M. Thelakkat, T.T. Albrecht, Effect of Chemical Modification on Molecular Ordering in Polydiketopyrrolopyrrole Copolymers: From Liquid Crystalline to Crystalline, Macromolecules 29 (2024) 5243. https://doi.org/10.1021/acs.macromol.4c00264.

[27] Z. Gan, L. Wang, J. Cai, C. Guo, C. Chen, D. Li, Y. Fu, B. Zhou, Y. Sun, C. Liu, J. Zhou, D. Liu, W. Li, T. Wang, Electrostatic force promoted intermolecular stacking of polymer donors toward 19.4% efficiency binary organic solar cells, Nature Communications 14 (2023) 6297. https://doi.org/10.1038/s41467-023-42071-2.

[28] S.O. Odoh, C.J. Cramer, D.G. Truhlar, L. Gagliardi, Quantum-Chemical Characterization of the Properties and Reactivities of Metal-Organic Frameworks, Chem. Rev. 115 (2015) 6051.

https://doi.org/10.1021/cr500551h.
[29] K.I.M-C. Ching, Impact of Alkyl-Based Side Chains in Conjugated Materials for Bulk Heterojunction Organic Photovoltaic Cells-A Review, Energies 16 (2023) 6639. https://doi.org/10.3390/en16186639.
[30] C. Lee, W. Yang and R.G. Parr, Development of the Colle-Salvetti correlation-energy formula into a functional of the electron density, Phys. Rev. B 37 (1988) 785. https://doi.org/10.1103/PhysRevB.37.785.
[31] M.J. Frisch and al, Gaussian 16, Revision C.01, Gaussian, Inc., Wallingford CT (2016).
[32] C. Lee, W. Yang, R.G. Parr, Development of the Colle-Salvetti correlation-energy formula into a functional of the electron density, Phys. Rev. B 37 (1988) 785. https://doi.org/10.1103/PhysRevB.37.785.
[33] A. Hlel, A. Mabrouk, M. Chemek, I. Ben Khalifa, K. Alimi, A DFT study of chargetransfer and opto-electronic properties of some new materials involving carbazole units, Computational Condensed Matter 3 (2015) 30. https://doi.org/10.1016/j.cocom.2015.02.001.
[34] N.M. O'Boyle, A.L. Tenderholt and K.M. Langner, A Library for Package-Independent Computational Chemistry Algorithms, J. Comp. Chem. 29 (2008) 839. http://dx.doi.org/10.1002/jcc.20823.
[35] C.-W. Chu, V. Shrotriya, G. Li, and Y. Yang, Tuning acceptor energy level for efficient charge collection in copper-phthalocyanine-based organic solar cells, Applied Physics Letters 88 (2006) 153504. https://doi.org/10.1063/1.2194207.
[36] H. Naz, M. Hussain, M. Adnan, R. Hussain, Z. Irshad , H. W. Darwish , U. Farooq , J. Yaqoob and J. Lim , Enhancing Optical and Optoelectronic Characteristics of Nonfused Ring-Containing Electron Acceptors for Efficient Organic Photovoltaics, J. Phys. Chem. C 129 **(**2025) 12204. https://doi.org/10.1021/acs.jpcc.5c03016.
[37] K. Pereira, W. Wu, L. You, J.F. Elman, Z. Wang, X. Wang, M. Ahmed, Z. Ke, J. Mei, Absorption Coefficient and Optical Contrast Modulation through Side Chain Engineering of Electrochromic Polymers, Macromolecules 56 (2023) 480. https://doi.org/10.1021/acs.macromol.2c02028.
[38] H. Bouazizi, A. Mabrouk, M.B. Braiek, T. Mestiri, K. Alimi, New conjugated organic matrix-carbon nanotube functionalization: DFT modeling and spectroscopic analysis, Journal of Physics and Chemistry of Solids 136 (2020) 109131. https://doi.org/10.1016/j.jpcs.2019.10913.
[39] Y. Liang, X. Deng, L. Zhang, X. Peng, W. Gao, J. Cao, Z. Gu, B. He, pH-responsive polymeric micelles with an acid-labile linkage for active tumor targeting and fast drug release, Biomaterials 71 (2015) 1. https://doi.org/10.1098/rsos.171654.
[40] H. Pham, R. Yan, J. McEachin, S. Zou, D. Zhang, Overcoming Subjectivity in Bandgap Evaluation through On-Resonance Fluorescence: Establishing a Robust and Objective, Optical Metric for Fluorescent Materials, ACS Meas Sci Au 6 (2026) 544. https://doi.org/10.1021/acsmeasuresciau.6c00017.
[41] W.-C. Chen, I. Chao , Molecular Orbital-Based Design of π-Conjugated Organic Materials with Small Internal Reorganization Energy: Generation of Nonbonding Character in Frontier Orbitals, J. Phys. Chem. C 118 (2014) 20176. https://doi.org/10.1021/jp5056655.
[42] E. Steiner, P.W. Fowler, R.W.A. Havenith, Current Densities of Localized and Delocalized Electrons in Molecules, J. Phys. Chem. A 106 (2002) 7048.

https://doi.org/10.1021/jp020819u.

[43] S. Zhou, X. Tao, Z. Liu, H. Wu, Z. Guan, L. Liu, J. Li, X. Chen and W. Ou-Yang, Regulation of Dihedral Angle on Molecular Engineering for Enhancing Triboelectric Performance, Adv. Funct. Mater. 34 (2024) 2405443. https://doi.org/10.1002/adfm.202405443.

[44] H. Naz, M. Hussain, M. Adnan, R. Hussain, Z. Irshad, H. W. Darwish, U. Farooq, J. Yaqoob and J. Lim, Enhancing Optical and Optoelectronic Characteristics of Nonfused Ring-Containing Electron Acceptors for Efficient Organic Photovoltaics, J. Phys. Chem. C 129 (2025) 12204. https://doi.org/10.1021/acs.jpcc.5c03016.

[45] Z. Khan, H.J. Alathlawi, K.H. Salem, S. M.K. A. Naqvi, I.H. Jaghdam, M.S. Soliman , T.H.A. Hasanin, S. Ali, H.N. Bhatti, R.A. Khera, Computational insights into phthalimide-core non-fullerene acceptors for next-generation organic solar cells, RSC Adv. 15 (2025) 31019. https://doi.org/10.1039/d5ra04527d.

[46] P.R. Varadwaj, H.M. Marques, A. Varadwaj, I. Grabowski, K. Yamashita, Molecular Electrostatic Surface Potential: A Predictive Framework for Noncovalent Interactions and Adsorption Characteristics in Molecular Entities, Int. J. Mol. Sci. 27 (2026) 3352. https://doi.org/10.3390/ijms27083352.

[47] O. Ostroverkhova, Organic Optoelectronic Materials: Mechanisms and Applications, Chem. Rev. 116 (2016) 13279. https://doi.org/10.1021/acs.chemrev.6b00127.

[48] C.F.N. Marchiori, M. Koehler, Dipole assisted exciton dissociation at conjugated polymer/fullerene photovoltaic interfaces: A molecular study using density functional theory calculations, Synthetic Metals 160 (2010) 643. https://doi.org/10.1016/j.synthmet.2009.12.026.

[49] M. Hallermann, S. Haneder, E. Da Como, Charge-transfer states in conjugated polymer/fullerene blends: Below-gap weakly bound excitons for polymer photovoltaics, Appl. Phys. Lett. 93 (2008) 053307. https://doi.org/10.1063/1.2969295.

[50] S.-I. Kiyooka, D. Kaneno, R. Fujiyama, Parr's index to describe both electrophilicity and nucleophilicity, Tetrahedron Letters 54 (2013) 342. https://doi.org/10.1016/j.tetlet.2012.11.039.

[51] M. Ibrahim, Molecular Modeling and FTIR Study for K, Na, Ca and Mg Coordination with Organic Acid, J. Comput. Theor. Nanosci. 6 (2009) 682. https://doi.org/10.1166/jctn.2009.1094.

[52] M.R. Gutiérrez, A.S. Sousa, L.R. Domingo, Electrophilicity and nucleophilicity scales at different DFT computational levels, Journal of Organic Physical Chemistry 36 (2023) e4503. https://doi.org/10.1002/poc.4503.

[53] L.R. Domingo, M.R. Gutiérrez, P. Pérez, Applications of the Conceptual Density Functional Theory Indices to Organic Chemistry Reactivity, Molecules 21 (2016) 748. https://doi.org/10.3390/molecules21060748.